The femtosecond structure of extreme contrast, multi-terawatt second-harmonic laser pulses at 400 nm

C. Aparajit, Ankit Dulat, Anandam Choudhary, Amit D Lad, Yash M Ved, Arnaud Couairon, G. Ravindra Kumar

RESEARCH ARTICLE | OCTOBER 04 2023

The femtosecond structure of extreme contrast, multi-terawatt second-harmonic laser pulses at 400 nm

C. Aparajit ; Ankit Dulat ; Anandam Choudhary ; Amit D. Lad ; Yash M. Ved ; Arnaud Couairon ; G. Ravindra Kumar

Appl. Phys. Lett. 123, 141108 (2023)
https://doi.org/10.1063/5.0174513

Applied Physics Letters ARTICLE pubs.aip.org/aip/apl

The femtosecond structure of extreme contrast, multi-terawatt second-harmonic laser pulses at 400 nm

Cite as: Appl. Phys. Lett. **123**, 141108 (2023); doi: 10.1063/5.0174513
Submitted: 31 August 2023 · Accepted: 18 September 2023 ·
Published Online: 4 October 2023

C. Aparajit,[1] Ankit Dulat,[1] Anandam Choudhary,[1] Amit D. Lad,[1] Yash M. Ved,[1] Arnaud Couairon,[2] and G. Ravindra Kumar[1,a)]

AFFILIATIONS

[1]Tata Institute of Fundamental Research, 1 Homi Bhabha Road, Colaba, Mumbai 400 005, India
[2]Centre de Physique Théorique, CNRS, Ecole Polytechnique, Institut Polytechnique de Paris, 91128 Palaiseau, France

[a)]Author to whom correspondence should be addressed: grk@tifr.res.in

ABSTRACT

Ultrahigh intensity contrast and short pulse laser–solid interactions offer an attractive platform for investigating high-energy-density matter, particularly in the context of structured and ultra-thin targets that form hot, dense plasma conditions. Harmonic generation can improve the contrast of laser pulses by several orders of magnitude. In this study, we present the characterization of extreme contrast, relativistic intensity second-harmonic pulses at 400 nm, using the self-diffraction frequency-resolved optical gating technique. The 400 nm pulses were generated at various input intensities using potassium dihydrogen phosphate and lithium triborate crystals. Our observations reveal the presence of spectral broadening, pulse compression, and complex structures at higher input intensities. We see that extreme contrast, few tens of femtosecond pulses can have multiple "prepulses" at the 100s femtosecond scale as large as ten percent of the peak value. These can preionize a solid significantly and may influence the interaction. Simulations based on nonlinear pulse propagation equations reinforce our findings.

The relentless march of ultrashort laser pulses to higher and higher peak intensities is sparking off rapid progress in high energy density science, with myriad applications, viz., generation of high brightness, ultrafast electromagnetic and material particle sources, laboratory simulation of astrophysical scenarios, application of extreme shocks to materials, etc.[1,2] Much of this physics is intrinsically nonlinear and is driven by femtosecond terawatt and petawatt laser pulses. An important demand these studies make on the laser pulses is the requirement of ultrahigh intensity contrast: the intensity away from the femtosecond main pulse on either side of the peak intensity to fall off to a very low value within a few picoseconds. There have been numerous recent works emphasizing the importance of ultrahigh contrast pulses, for example, the generation of homogenous high-energy density matter,[3] electron and ion acceleration from ultra-thin targets, using structured targets for creating hot, dense plasma conditions, and hence high flux, electromagnetic, and material particle emission[4–9] where the contrast becomes essential for preserving the structure.

One effective approach to enhance contrast involves nonlinear modification of the laser pulse, often utilizing second harmonic generation (SHG) to achieve extreme contrast pulses.[3,4,7,10–13] While SHG plays a role in enhancing laser contrast, the intensity profile and instantaneous temporal/spectral phase of the pulse in the femtosecond regime are of utmost importance in laser–matter interactions. While attention is often placed on the impact of picosecond pedestals and nanosecond contrast, the presence of a femtosecond structure within the temporal profile holds equal, if not greater, significance in laser–matter interactions. To measure the instantaneous phase, two commonly employed methods are frequency-resolved optical gating (FROG)[14] and spectral phase interferometry for direct electric-field reconstruction (SPIDER).[15] Commercial devices are readily available for measuring the instantaneous phase of the 800 nm pulses produced by high-power Ti-Sapphire lasers. However, there is a scarcity of reports regarding such measurements at the second harmonic (400 nm), particularly at terawatt or higher peak powers. Most laser systems report these measurements at a preliminary stage during the amplification process, and as demonstrated below, unusual effects on the pulse shape can occur at high powers.

In a recent study, we demonstrated high-efficiency second harmonic conversion of an 800 nm pulse using a lithium borate (LBO) crystal, resulting in the generation of relativistic intensity laser pulses

at 400 nm.[16] In this paper, we provide a complete temporal characterization of the second harmonic pulse generated from both type-1 lithium triborate (LBO) and type-1 potassium dihydrogen phosphate (KDP) crystals using the self-diffraction geometry of frequency-resolved optical gating (SD-FROG). We show that at multi-terawatt input (800 nm) peak powers, the SH pulse exhibits spectral broadening, pulse width compression, and a complex structure. Significantly, we notice the presence of prepulses at the 100s of the femtosecond level, with strength as large as 10%–15% of the peak value, which may seriously modify the interaction of a few tens of femtosecond pulse with a solid. These features can be attributed to second and higher-order nonlinearities within the SHG crystal, and it is essential to consider them when modeling the pulse's interaction with matter. We present simulations involving nonlinear pulse propagation to explain our results. The measurements and outcomes presented in our study hold significant value and interest for the scientific community, particularly given the increasing interest in the utilization of extremely high contrast pulses.

We present data for two crystals, KDP and LBO, both of which are important in the high-intensity regime of SHG. KDP is the more common option used in petawatt class laser systems due to their ease of growth of large-aperture crystals, wideband phase matching at 800 nm input wavelength, and not to forget their lower cost. It is only recently that large-size LBO crystals have become available and interestingly report much higher SHG conversion efficiencies.[16] It is likely LBO will be explored more in the future and can become a strong contender for SHG in petawatt class laser systems. Temporal structures depend strongly on the dispersion and nonlinear properties of the crystals; thus, it is important to experimentally measure and study their impact on the temporal structure of SH pulses from both these crystals. Here, we report the experimental measurements and highlight the temporal features (an earlier numerical study had hinted at pulse structure in KDP).[17]

The experiment was conducted using a chirped pulse amplified 150 TW Ti:sapphire laser system delivering 800 nm, 27 fs, and 50 nm bandwidth pulses at a 5 Hz repetition rate. The laser was well stabilized (shot-to-shot energy fluctuations was $< \pm 5\%$) before the measurements. The 800 nm pulses were up-converted inside a vacuum chamber (10^{-6} Torr) to 400 nm using two separate SH crystals, a 70 mm diameter, 2 mm thick type-I lithium triborate (LBO) crystal (Cristal Laser) and a 50 mm diameter, 1 mm thick, type-I potassium dihydrogen phosphate (KDP) crystal (EKSMA Optics). Figure 1(a) shows the contrast profiles for our 800 nm pulses, measured using SEQUOIA (Amplitude Technologies)—a third-order cross correlator[18,19] and the theoretical estimates for the 400 nm pulses. Also, our input pulses are p-polarized, and the SH pulses are s-polarized, measured using an analyzer/polarizer setup.

A standard multi-shot SD-FROG setup[14] was built for the 400 nm pulse characterization. For a detailed description of the setup, see Fig. S1 and section 1 of the supplementary material.

There are earlier reports of SD-FROG measurements done using 1 mm quartz as the nonlinear medium.[20] Recent two-photon absorption measurements using beta-phase gallium oxide (β-Ga_2O_3) indicate its strong third-order nonlinearity around UV and visible wavelength spectral range,[21,22] making beta-phase gallium oxide a really promising candidate as a nonlinear medium for SD-FROG measurements. We used a (100) beta-phase gallium oxide, with a thickness of about 100 μm, grown using the optical floating zone technique.

The spectra of the SH pulses from the LBO crystal for different input energies are shown in Fig. 1(b). We note that the bandwidth of the spectra increases with input energy and the spectra develop additional modulations, which are known to arise from higher-order nonlinearities like self-phase modulation.[17,23] The bandwidth increases from nearly 1.5 nm at lower energy to about 10 nm at highest energy taking into account the extra wings in the spectra.

The SD FROG traces are shown in Figs. 2 and 3, which are obtained for four different cases of input energy and SH crystals, i.e., 130 mJ (~0.11 TW/cm^2) and 1300 mJ (~1.1 TW/cm^2), on the LBO crystal, and 80 mJ (~0.12 TW/cm^2) and 600 mJ (~0.9 TW/cm^2) on the KDP crystal. Considering the difference in diameter (LBO—70 mm diameter and KDP—50 mm diameter), the effective intensities on the two crystals are similar at the two lower and higher energy cases. In the lower-intensity case, we see a clean, near transform-limit, FROG trace with a slight chirp. The higher-intensity case, on the other hand, has significant distortions involving spectral and temporal modulations in the trace. Also note, at the highest intensity used in the experiments, the B-integral for the pump beam is in the range of $0.5-1\pi$, which is below the value for small-scale self-focusing (SSSF) to be significant. The beam profiles were smooth, and microscopic examinations of the SH crystals showed no indications of damage, gray tracking, or degeneration of the crystals after multiple runs of the experiment.[16]

The complex electric fields and phase information are determined by using the following self-diffraction non-linearity in a generalized projections based phase retrieval algorithm:[14]

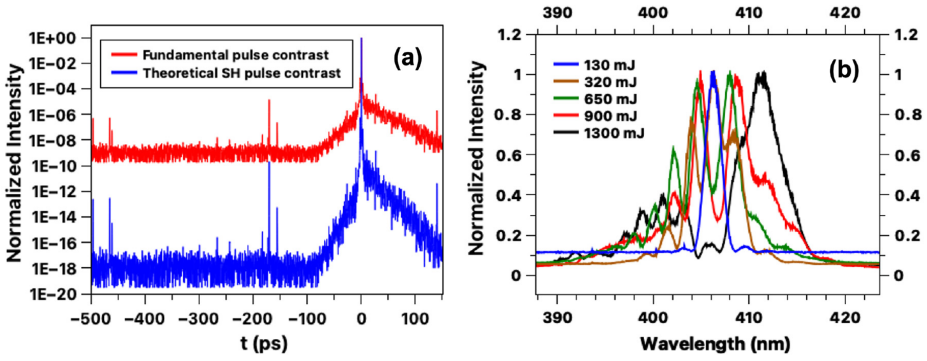

FIG. 1. (a) Laser contrast of input pulse and the expected contrast of the SH pulse and (b) spectrum of 400 nm pulses for different input energies on the LBO crystal.

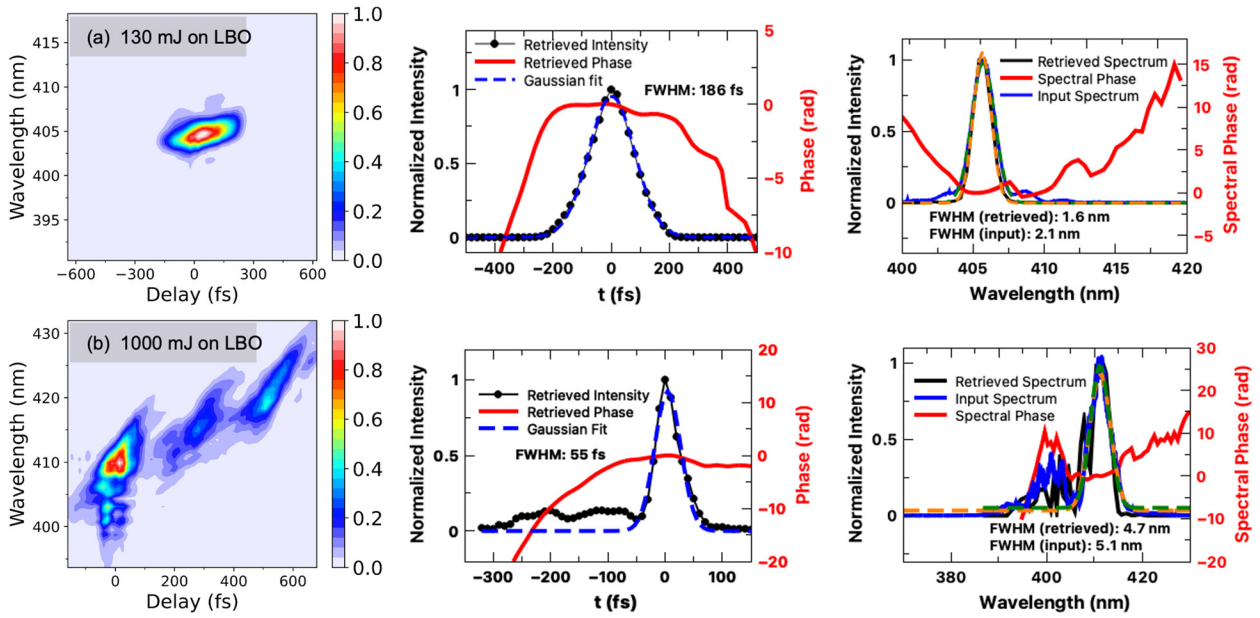

FIG. 2. Compilation of SD FROG traces, retrieved pulse, and spectrum for two cases of input energy, i.e., (a) 130 and (b) 1000 mJ on the LBO crystal. The dashed lines in each spectrum correspond to Gaussian fits (orange dashed for input spectra and green dashed for retrieved spectra).

$$I^{SD}_{FROG}(\omega,\tau) = \left| \int_{-\infty}^{\infty} E(t)^2 E(t-\tau)\, \exp(-i\omega t) dt \right|^2.$$

First, we consider the SH profiles from the LBO crystal. Figures 2(a) and 2(b) show the retrieved intensity and spectrum for the two extreme cases, i.e., 130 and 1300 mJ, on the LBO crystal. For the lower energy case of 130 mJ, we see a near-perfect Gaussian fit to the intensity profile with a pulse width of 186 fs. The beam traveled through roughly 10 mm of fused silica, 8 mm while exiting the vacuum chamber, and 2 mm in the lenses of the SD FROG setup. So, compensating

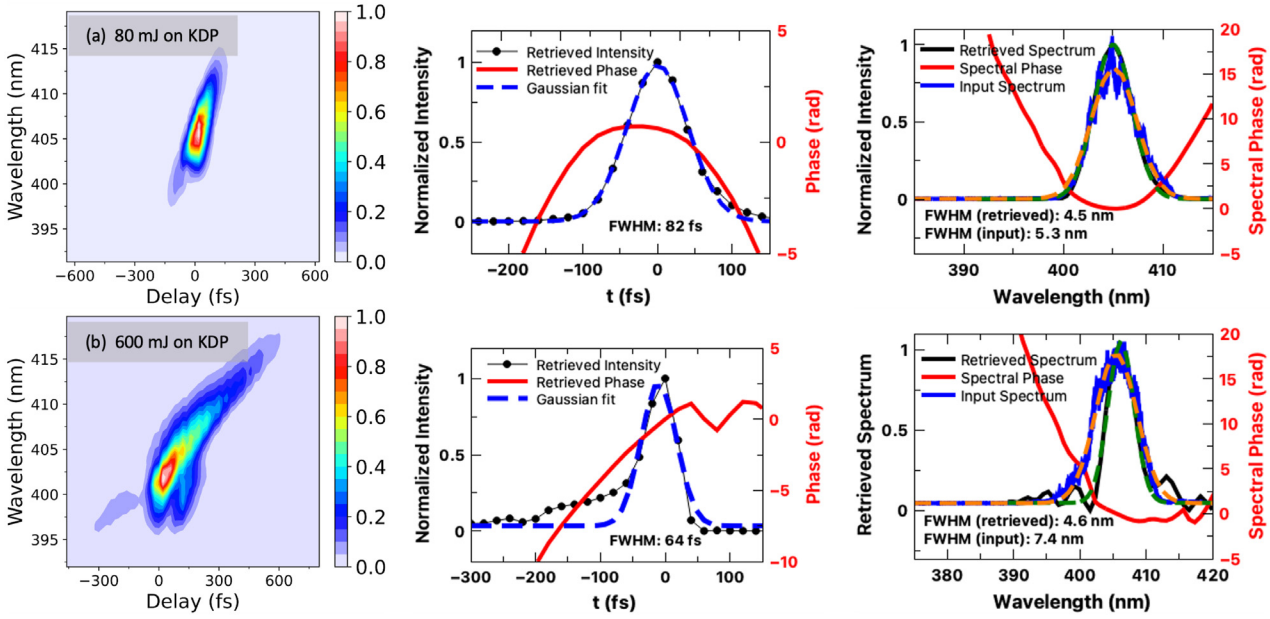

FIG. 3. Compilation of SD FROG traces, retrieved pulse, and spectrum for two cases of input energy, i.e., (a) 80 and (b) 600 mJ on KDP crystal. The dashed lines in each spectrum correspond to Gaussian fits (orange dashed for input spectra and green dashed for retrieved spectra).

for the group-velocity dispersion (GVD) for 400 nm pulses traveling through 10 mm of FS, the pulse width does not change significantly and remains similar to 185 fs. The retrieved spectrum also matches the input 400 nm spectrum entering the SD FROG setup and has a bandwidth of about 1.6 nm. The transform limit for a 1.6 nm bandwidth, 400 nm pulse comes out to be ∼150 fs, and so our pulse width is slightly greater than that, which is expected from the slight tilt in the FROG trace and also the quadratic chirp in the spectral phase. On the other hand, the higher energy case of 1300 mJ has significant "pre-pulse" structures before the main pulse, whose strength is as large as 10%–15% of the peak. Performing a Gaussian fit to the main peak yields a pulse width of about 55 fs, but in essence, the 55 fs pulse must be considered as large as nearly 300 fs temporal span for modeling the interaction. The femtosecond structures are being highlighted in Fig. 2(b) [and also Fig. 3(b)]. The retrieved spectrum also has extra structures on the left, which is also seen in the input spectrum. The bandwidth of the main spectral peak is 4.7 nm in the retrieved case and 5.1 nm in the input spectrum. It is known that the phase mismatch in a nonlinear process is in general wavelength dependent. For a large bandwidth pulse especially, the SD process can introduce wavelength-dependent effects into the trace, leading to distortions in the trace and retrieved pulse. However, we have kept the bare minimum energy on gallium oxide to reduce these measurement artifacts. The extra structures are due to the nonlinear properties of the crystal, as will also be clear from the simulations.

Second, we consider the SH profiles from the KDP crystal. Figures 3(a) and 3(b) show the FROG traces, retrieved intensity profile, and the spectra for 80 and 600 mJ on the KDP crystal, respectively. Our 80 mJ FROG trace has a tilt, which corresponds to a negative chirp, which is also seen from the quadratic temporal phase in the retrieved intensity profile. Also, for the low energy case, the pulse width is seen to be 82 fs. The measured spectral bandwidth is about 4.5 nm and the retrieved one is 5.3 nm, and they are quite in agreement. Also, the quadratic spectral phase implies a temporal broadening from the transform limit. For the higher energy case, the trace is stretched along the wavelength axis and shorter along the delay axis. Modulations in the trace introduce a side hump or a ramp-link structure in the temporal profile. A Gaussian fit to the main fs peak gives a pulse width of 64 fs, but the effective pulse width is slightly larger due to the extra structures. The input and retrieved spectra show slight deviations, with the input bandwidth being 7.4 nm and the retrieved bandwidth being 4.6 nm. In comparison with an LBO crystal, KDP has lower linear dispersion values, i.e., both group-velocity mismatch (GVM) and group-velocity dispersion (GVD), and hence leads to shorter pulses and broader spectra. However, it has a lower second-order nonlinearity that leads to lower second-harmonic conversion efficiencies. It also has an order of magnitude higher third-order nonlinearity leading to temporal and spectral modulations at a lower threshold input fluence.

The simulation model (adapted from Refs. 24 and 25) is detailed in Ref. 16 and also in section 2 of the supplementary material. It describes the propagation of the laser pulse envelopes at the fundamental and SH frequencies and takes into account (i) non-uniformity of the beams, (ii) the effect of phase and GVM, (iii) GVD, (iv) quadratic, and (v) Kerr nonlinearities. The parameters for the crystals were all taken from Refs. 23 and 26–28.

The simulation results for the LBO crystal are shown in Fig. 4. Figure 4(a) shows the temporal profile, and Fig. 4(b) the spectra obtained for two cases of input energy, which were taken according to the experimental conditions. First, regarding the temporal pulse width, we obtain an FWHM (from a Gaussian fit) of about 174 fs for the low energy case and an FWHM of about 70 fs for the higher energy case. This is in good agreement with experiments. Second, the spectra also show a significant spectral broadening at higher input energies. We also ran the simulation by turning the third-order nonlinearity off, to see just the effect of the SHG process on the pulse propagation. These are presented in the blue curves in Fig. 4. These exhibit the fact that the pulse compression aspect is predominantly due to the SHG process, and the third-order term then stretches this pulse further. However, spectral broadening is mainly due to the third-order effects.

Figure 5(a) shows the temporal shape of the SH pulse for the case of 100 mJ of input energy, whereas Figs. 5(b) and 5(c) show the corresponding temporal and spectral shapes of the SH pulse for the higher energy case of 1 J of input 800 nm pulse energy on the LBO crystal. Initially, the pulse width is similar to the input 800 nm pulse width, i.e., 25 fs, but as the pulse propagates through the crystal, the dispersive effects of the crystal lead to pulse stretching. The spectral bandwidth is higher at 0.5 mm distance vs 2 mm distance traveled in the crystal, which is attributed to the phase mismatch. Also, third-order effects lead to the spectral modulations seen later. We should note that 0.5 mm thickness produces the broadest spectrum and shortest pulse without complex structure and still produces good conversion efficiencies (see Fig. S2 in the supplementary material). However, due to the requirement of large diameter crystals, 2 mm is preferable for

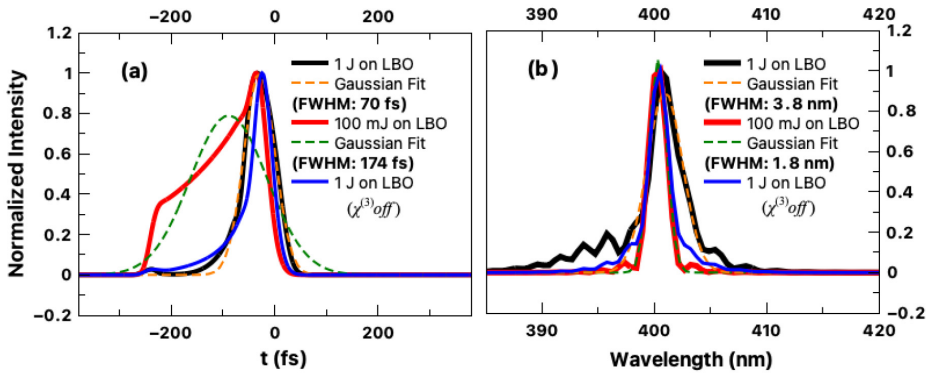

FIG. 4. Results from the nonlinear pulse propagation simulations. (a) Temporal profiles and (b) spectra for the two cases of 130 and 1300 mJ input energy on the LBO crystal.

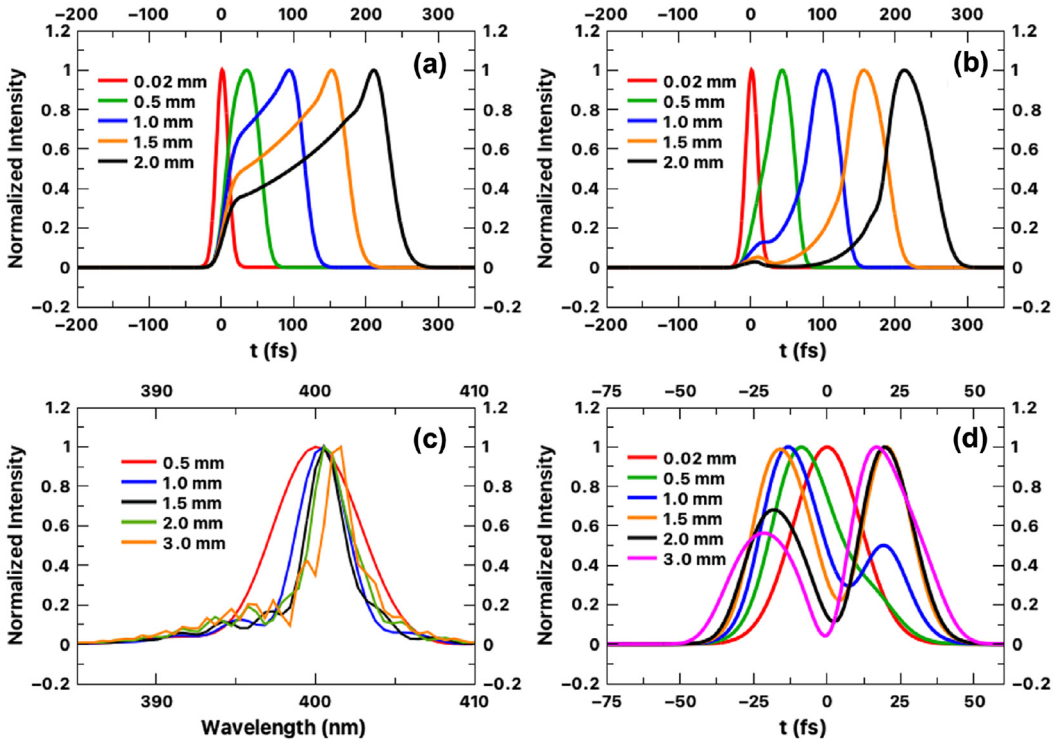

FIG. 5. Temporal shape evolution of the SH pulses as a function of the distance traveled in the LBO crystal for (a) 100 mJ input energy on LBO, (b) 1 J input energy on LBO, (c) spectral shape evolution for the higher input energy case, and (d) the corresponding shape of the fundamental pulse.

mechanical stability without compromising too much on temporal shapes. Figure 5(d) corresponds to the fundamental pulse shapes as it propagates through the crystal for the higher energy case. We notice that the pulse shapes split into two parts after 1 mm of travel. This, along with the GVM between the fundamental and SH pulses, leads to the extra structure in SH temporal profiles starting from 1 mm travel [see Fig. 5(b)]. The double hump structure in 800 nm pulse thus explains the modulations in temporal and spectral modulations in the SH pulse as seen in both simulations and experiments.

To conclude, we report the spectrum and pulse characteristics for extreme contrast 400 nm pulses produced using LBO and KDP crystals at input intensities of $\sim$ TW/cm^2. At higher input intensities, we observe significant spectral broadening and pulse compression of the 400 nm pulses owing to the SHG process and higher-order nonlinearities, especially the third-order processes like self-phase and cross-phase modulations. The effect of pulse compression is useful in reaching higher intensities and producing more extreme high-energy-density states in relativistic laser–matter interactions. A notable finding is the occurrence of strong prepulse structures at the 100s of the femtosecond scale for a tens of femtosecond duration pulse. In petawatt class laser systems, efficient SHG will inherently have such femtosecond temporal structures due to dispersion and cubic nonlinearities in the SHG crystals, which may be unavoidable due to several constraints (like minimum thickness necessary to ensure mechanical stability of large transverse size crystals, in turn, necessitated by the large petawatt beam sizes *and* to reduce the B integral). It is thus absolutely imperative to consider such modifications to the temporal structure in order to realistically understand the physics of the interaction. This should be accounted for in modeling the interaction of such pulses with solids.

See the supplementary material for the schematic of the experimental setup, a detailed description of the measurements, simulation details based on nonlinear pulse propagation equations, and some additional results from simulations.

G.R.K. acknowledges J. C. Bose Fellowship Grant (No. JBR/2020/000039) from the Science and Engineering Board (SERB), Government of India. A.D.L. acknowledges partial support from the Infosys-TIFR Leading Edge Research Grant (Cycle 2). We thank Maneesha Narayanan and Professor Arnab Bhattacharya (TIFR, Mumbai) for providing the (100) beta phase-gallium oxide sample for the SD-FROG measurements. We also thank Professor Rick Trebino and Dr. Rana Jafari (Georgia Tech) for providing the SD-FROG pulse retrieval codes.

AUTHOR DECLARATIONS

Conflict of Interest

The authors have no conflicts to disclose.

Author Contributions

C. Aparajit: Formal analysis (lead); Investigation (lead); Methodology (lead); Software (lead); Validation (lead); Writing – original draft (lead); Writing – review & editing (lead). **Ankit Dulat:** Investigation

(equal); Methodology (equal); Writing – review & editing (supporting). **Anandam Choudhary:** Investigation (equal); Methodology (equal); Writing – review & editing (supporting). **Amit D. Lad:** Funding acquisition (supporting); Investigation (equal); Methodology (equal); Resources (lead); Writing – review & editing (supporting). **Yash M. Ved:** Resources (equal); Writing – review & editing (supporting). **Arnaud Couairon:** Software (equal); Supervision (equal); Writing – review & editing (equal). **G. Ravindra Kumar:** Conceptualization (lead); Funding acquisition (lead); Supervision (lead); Writing – original draft (lead); Writing – review & editing (lead).

DATA AVAILABILITY

The data that support the findings of this study are available from the corresponding author upon reasonable request.

REFERENCES

[1]R. P. Drake, *High Energy Density Physics* (Springer-Verlag, Berlin, Heidelberg, 2006).
[2]P. K. Kaw, "Nonlinear laser–plasma interactions," Rev. Mod. Plasma Phys. **1**, 2 (2017).
[3]N. F. Beier, H. Allison, P. Efthimion, K. A. Flippo, L. Gao, S. B. Hansen, K. Hill, R. Hollinger, M. Logantha, Y. Musthafa, R. Nedbailo, V. Senthilkumaran, R. Shepherd, V. N. Shlyaptsev, H. Song, S. Wang, F. Dollar, J. J. Rocca, and A. E. Hussein, "Homogeneous, micron-scale high-energy-density matter generated by relativistic laser-solid interactions," Phys. Rev. Lett. **129**, 135001 (2022).
[4]M. A. Purvis, V. N. Shlyaptsev, R. Hollinger, C. Bargsten, A. Pukhov, A. Prieto, Y. Wang, B. M. Luther, L. Yin, S. Wang, and J. J. Rocca, "Relativistic plasma nanophotonics for ultrahigh energy density physics," Nat. Photonics **7**, 796–800 (2013).
[5]A. Macchi, "Surface plasmons in superintense laser-solid interactions," Phys. Plasmas **25**, 031906 (2018).
[6]P. P. Rajeev, P. Taneja, P. Ayyub, A. S. Sandhu, and G. R. Kumar, "Metal nanoplasmas as bright sources of hard x-ray pulses," Phys. Rev. Lett. **90**, 115002 (2003).
[7]C. Bargsten, R. Hollinger, M. G. Capeluto, V. Kaymak, A. Pukhov, S. Wang, A. Rockwood, Y. Wang, D. Keiss, R. Tommasini, R. London, J. Park, M. Busquet, M. Klapisch, V. N. Shlyaptsev, and J. J. Rocca, "Energy penetration into arrays of aligned nanowires irradiated with relativistic intensities: Scaling to terabar pressures," Sci. Adv. **3**, e1601558 (2017).
[8]S. Kahaly, S. K. Yadav, W. M. Wang, S. Sengupta, Z. M. Sheng, A. Das, P. K. Kaw, and G. R. Kumar, "Near-complete absorption of intense, ultrashort laser light by sub-λ gratings," Phys. Rev. Lett. **101**, 145001 (2008).
[9]A. D. Lad, Y. Mishima, P. K. Singh, B. Li, A. Adak, G. Chatterjee, P. Brijesh, M. Dalui, M. Inoue, J. Jha, S. Tata, M. Trivikram, M. Krishnamurthy, M. Chen, Z. M. Sheng, K. A. Tanaka, G. R. Kumar, and H. Habara, "Luminous, relativistic, directional electron bunches from an intense laser driven grating plasma," Sci. Rep. **12**, 16818 (2022).
[10]D. F. Price, R. M. More, R. S. Walling, G. Guethlein, R. L. Shepherd, R. E. Stewart, and W. E. White, "Absorption of ultrashort laser pulses by solid targets heated rapidly to temperatures 1–1000 eV," Phys. Rev. Lett. **75**, 252–255 (1995).
[11]L. M. Chen, M. Kando, M. H. Xu, Y. T. Li, J. Koga, M. Chen, H. Xu, X. H. Yuan, Q. L. Dong, Z. M. Sheng, S. V. Bulanov, Y. Kato, J. Zhang, and T. Tajima, "Study of x-ray emission enhancement via a high-contrast femtosecond laser interacting with a solid foil," Phys. Rev. Lett. **100**, 045004 (2008).
[12]A. Saemann, K. Eidmann, I. E. Golovkin, R. C. Mancini, E. Andersson, E. Förster, and K. Witte, "Isochoric heating of solid aluminum by ultrashort laser pulses focused on a tamped target," Phys. Rev. Lett. **82**, 4843–4846 (1999).
[13]R. Hollinger, S. Wang, Y. Wang, A. Moreau, M. G. Capeluto, H. Song, A. Rockwood, E. Bayarsaikhan, V. Kaymak, A. Pukhov, V. N. Shlyaptsev, and J. J. Rocca, "Extreme ionization of heavy atoms in solid-density plasmas by relativistic second-harmonic laser pulses," Nat. Photonics **14**, 607–611 (2020).
[14]D. J. Kane and R. Trebino, "Characterization of arbitrary femtosecond pulses using frequency-resolved optical gating," IEEE J. Quantum Electron. **29**, 571–579 (1993).
[15]C. Iaconis and I. A. Walmsley, "Spectral phase interferometry for direct electric-field reconstruction of ultrashort optical pulses," Opt. Lett. **23**, 792–794 (1998).
[16]C. Aparajit, K. Jana, A. D. Lad, Y. M. Ved, A. Couairon, and G. R. Kumar, "Efficient second-harmonic generation of a high-energy, femtosecond laser pulse in a lithium triborate crystal," Opt. Lett. **46**, 3540–3543 (2021).
[17]S. Y. Mironov, V. V. Lozhkarev, V. N. Ginzburg, I. V. Yakovlev, G. Luchinin, A. Shaykin, E. A. Khazanov, A. Babin, E. Novikov, S. Fadeev, A. M. Sergeev, and G. A. Mourou, "Second-harmonic generation of super powerful femtosecond pulses under strong influence of cubic nonlinearity," IEEE J. Sel. Top. Quantum Electron. **18**, 7–13 (2012).
[18]R. C. Eckardt and C. H. Lee, "Optical third harmonic measurements of subpicosecond light pulses," Appl. Phys. Lett. **15**, 425–427 (1969).
[19]G. Albrecht, A. Antonetti, and G. Mourou, "Temporal shape analysis of Nd^{3+}: YAG active passive model-locked pulses," Opt. Commun. **40**, 59–62 (1981).
[20]T. S. Clement, A. J. Taylor, and D. J. Kane, "Single-shot measurement of the amplitude and phase of ultrashort laser pulses in the violet," Opt. Lett. **20**, 70–72 (1995).
[21]H. Chen, H. Fu, X. Huang, J. A. Montes, T.-H. Yang, I. Baranowski, and Y. Zhao, "Characterizations of the nonlinear optical properties for (010) and ($\bar{2}$ 01) beta-phase gallium oxide," Opt. Express **26**, 3938–3946 (2018).
[22]N. Zhang, I. M. Kislyakov, C. Xia, H. Qi, J. Wang, and H. F. Mohamed, "Anisotropic luminescence and third-order electric susceptibility of mg-doped gallium oxide under the half-bandgap edge," Opt. Express **29**, 18587–18600 (2021).
[23]T. Ditmire, A. M. Rubenchik, D. Eimerl, and M. D. Perry, "Effects of cubic nonlinearity on frequency doubling of high-power laser pulses," J. Opt. Soc. Am. B **13**, 649–655 (1996).
[24]J. Moses and F. W. Wise, "Controllable self-steepening of ultrashort pulses in quadratic nonlinear media," Phys. Rev. Lett. **97**, 073903 (2006).
[25]I. A. Begishev, M. Kalashnikov, V. Karpov, P. Nickles, H. Schönnagel, I. A. Kulagin, and T. Usmanov, "Limitation of second-harmonic generation of femtosecond Ti: Sapphire laser pulses," J. Opt. Soc. Am. B **21**, 318–322 (2004).
[26]D. N. Nikogosyan, "Lithium triborate (LBO)," Appl. Phys. A **58**, 181–190 (1994).
[27]S. Lin, Z. Sun, B. Wu, and C. Chen, "The nonlinear optical characteristics of a LiB_3O_5 crystal," J. Appl. Phys. **67**, 634–638 (1990).
[28]H. Li, F. Zhou, X. Zhang, and W. Ji, "Bound electronic Kerr effect and self-focusing induced damage in second-harmonic-generation crystals," Opt. Commun. **144**, 75–81 (1997).